Shallow Thermocline Bias in the Southern Tropical Pacific in CMIP5/6 Models

Maya Samuels[1], **Ori Adam**[1], **Hezi Gildor**[1]

[1]Fredy and Nadine Herrmann Institute of Earth Sciences, Hebrew University, Jerusalem, Israel

Key Points:

- Shallow thermocline bias across the southern tropical Pacific in CMIP5/6 models
- Double ITCZ and shallow thermocline biases are closely related
- Shallow southern thermocline bias linked to wider double ITCZ and stronger equatorial cold tongue

Corresponding author: Ori Adam, ori.adam@mail.huji.ac.il

Abstract

A basin-wide significant shallow bias is found in the southern tropical Pacific thermocline in an ensemble of models from the coupled model intercomparison project phases 5 and 6. In contrast to observations, where the southern thermocline is far deeper than its northern counterpart, models have a hemispherically symmetric tropical thermocline. The shallow thermocline bias is closely related to the well known double intertropical convergence zone (ITCZ) bias, as shown by ensemble partitioning. The physical thermocline (i.e., depth of maximal vertical thermal gradient) is more strongly linked to the double ITCZ bias than the commonly used 20°C isotherm thermocline proxy. A shallow thermocline bias is further found to be associated with wider separation of double ITCZ peaks, stronger southern precipitation, a stronger cold tongue, and a spurious south equatorial counter current. Climatic implications and feedback mechanisms between the biases are discussed.

Plain Language Summary

In this study we find that in global climate model simulations the depth of the tropical south Pacific thermocline is shallower than in reality. The thermocline is the layer that separates the warm upper ocean from its cold depths. When the thermocline is shallower, the capacity of the upper ocean to absorb heat from the atmosphere is reduced. This means that the error in the modeled depth of the thermocline could alter the modeled heat balance between the ocean and atmosphere, as well as the heat imbalance between the northern and southern hemispheres. We further find that a well known error of excessive rain in the tropical south Pacific, which has been a major problem in models for the past three decades and remains unsolved, is worse in models that have this thermocline simulation problem. By drawing connections between the two model inaccuracies, progress can be made in understanding their sources. Correcting the thermocline simulation error and the errors associated with it is critical to the reliability of global scale model predictions.

1 Introduction

The thermocline is the layer in the ocean of maximal temperature decline. It separates the upper ocean, where air-sea interactions occur, from the abyssal ocean, affording the two regions distinct circulations, thermodynamic properties and characteristic timescales (Knauss & Garfield, 2016). Impacts of thermocline depth on the climate system are diverse and fundamental. In particular, it influences sea surface temperature (SST) by setting the thermal foot-

print of Ekman divergence driven upwelling. Such is the case, for example, along the equatorial Pacific and Atlantic cold tongues, where a strip of cold surface water extends from the east due to zonal sloping of the thermocline (Sverdrup et al., 1942). Thermocline depth also regulates ocean heat storage, ocean energy transport and, by extension, the global energy budget (Boccaletti et al., 2004; Vialard et al., 2001; Schott et al., 2004). Since thermocline depth marks the lower boundary of the ocean layer most susceptible to mechanical and radiative forcing, its representation in climate models is paramount (Harper, 2000; Burls et al., 2017; Thomas & Fedorov, 2017).

Models participating in phases 3 and 5 of the Coupled Model Intercomparison Project (CMIP) are known to systematically produce a too shallow equatorial thermocline (e.g., Zheng et al., 2012; Li & Xie, 2012, 2014; Castaño-Tierno et al., 2018). However, the meridional structure of the tropical thermocline and its relation to the intertropical convergence zone (ITCZ, a zonal band near the equator where tropical rain is concentrated) has not been fully investigated in coupled General Circulation Models (GCMs). Tropical Pacific meridional thermocline structure is particularly interesting in light of the well known double ITCZ bias (DIB), characterized by excessive precipitation south of the equator primarily in the Pacific (Fig. 1a–c; Mechoso et al., 1995; Lin, 2007; Adam, Schneider, & Brient, 2018). A DIB is often accompanied by a cold-tongue bias, where the modeled cold tongue is too cold and westward extended (Li & Xie, 2014). Coupled ocean-atmosphere dynamics have been shown to be at the root of the DIB, but the source of the bias remains unknown.

In the tropics, a warm well-mixed surface layer typically sits above a strong thermocline year-round (Knauss & Garfield, 2016). A strong or stable thermocline (i.e., a layer of large vertical thermal gradient, $\partial_z \theta$) forms a barrier that weakens mixing between the upper and abyssal layers and is often shallower and thinner (Vallis, 2017). Thermocline depth may be shoaled by modulation of the diffusivity of heat downward and advection of cold water upwards between the abyssal and upper layers, but also by surface warming or abyssal cooling through increased stratification (Vallis, 2017). Wind driven Ekman transport is pivotal to thermocline structure as well: subtropical current convergence causes subduction and thermocline deepening; current divergence at the equator, along eastern coastlines and near the ITCZ, causes upwelling and thermocline shoaling (Luyten et al., 1983). In the limit of geostrophy, the thermocline shoals to the left (right) of ocean currents when facing downstream in the northern (southern) hemisphere (Knauss & Garfield, 2016). A shallow thermocline is expected to be

more reactive to surface processes such as wind stress and radiative changes on seasonal and inter-annual timescales.

In this paper we study the tropical Pacific thermocline in an ensemble of CMIP phases 5 and 6 (CMIP5/6) models. Comparison with reanalysis data reveals a significant shallow bias in the southern tropical Pacific thermocline. Section 2 describes the data and diagnostics. In section 3 we characterize the shallow thermocline bias. We then examine tropical influences of the bias in section 4 and end in section 5 with a discussion of possible sources and implications, as related to the double ITCZ and cold tongue problems.

2 Data and Methods

2.1 Data

For oceanic reference data, we used the European Center for Medium-range Weather Forecasts Ocean Reanalysis/Analysis System phases 4 and 5 (ORAS4/5) (Zuo et al., 2019), the Global Ocean Data Assimilation System (GODAS) (Behringer & Xue, 2004) and the Simple Ocean Data Assimilation version 3.12.2 (SODA3) reanalysis (Carton et al., 2018). Precipitation data was taken from the National Oceanic and Atmospheric Administration's (NOAA) Global Precipitation Climatology Project (GPCP), version 2.2 (Adler et al., 2003) and from the Climate Prediction Center (CPC) Merged Analysis of Precipitation (CMAP) (P. Xie & Arkin, 1996). SST data was taken from version 3b of the Extended Reconstructed SST (ERSST.v3b) dataset, provided by NOAA's National Climatic Data Center (Smith et al., 2008). For model data, we analyzed 37 CMIP5 and 36 CMIP6 models (see Tables T1/2), based on availability. We used monthly data from the first realization of historical simulations (coupled GCMs driven by prescribed atmospheric compositions). All analyses were performed on monthly climatology computed between 1979–2005.

2.2 Diagnostics

Thermocline Depth Estimation

Due to sparse ocean measurements and low vertical ocean model resolution, thermocline depth is commonly approximated as an isotherm (Fiedler, 2010). In the tropical Pacific, the 20°C isotherm (Z20) has been used widely in observational and model analyses (e.g., Zheng et al., 2012; Li & Xie, 2012)). However, important distinctions exist between the depth of the physical thermocline (i.e., depth of maximal $\partial_z \theta$, denoted here as Ztc) and isothermal defi-

nitions, especially in their sensitivity to tropical mechanical forcing. Specifically, Z20 tends to be deeper, flatter and less sensitive to seasonal warming (Castaño-Tierno et al., 2018). Therefore, in the present study we look at both Ztc and Z20.

Z20 is computed through linear interpolation of ocean potential temperature (Castaño-Tierno et al., 2018). Ztc is calculated using

$$\mathrm{Ztc} = \frac{\int_{z_t}^{z_b} (\partial_z \theta)^n z dz}{\int_{z_t}^{z_b} (\partial_z \theta)^n dz} \tag{1}$$

where subscripts t and b denote top and bottom depths, respectively, and $\partial_z \theta$ is the vertical gradient of the potential temperature calculated between each two consecutive levels. This reduces grid dependence, where n acts as a smoothing parameter, such that for n = 1, Ztc is the depth of the centroid of $\partial_z \theta(z)$, and for $n \to \infty$, Ztc is the depth of the exact half-grid local maximum with no smoothing (Adam, Grise, et al., 2018). We took z_t to be the average of the upper two levels ($\sim$ 10 meters in most datasets), z_b as the average of the two levels closest to 400 meters in each dataset, and a smoothing factor of n=15. Results are not sensitive to either parameter.

Tropical Asymmetry Index

The tropical Pacific asymmetry index A_f (Hwang & Frierson, 2013) of a field f zonally averaged within the Pacific (160–260°), is defined as the (area-weighted) north-tropical average (0–20°N) minus the south-tropical average (0–20°S), normalized by the tropical average (20°S–20°N):

$$A_f = \frac{\bar{f}_{0-20\mathrm{N}} - \bar{f}_{20\mathrm{S}-0}}{\bar{f}_{20\mathrm{S}-20\mathrm{N}}}. \tag{2}$$

A_f is positive if f is greater north of the equator than south, negative if f is greater south of the equator than north, and zero if the distribution is symmetric about the equator.

3 Thermocline Biases

Thermocline depth (Ztc) is shown in Fig. 1a for the ORAS5 reanalysis. Tropical Pacific deepening is the most prominent feature, found between 10° and 20° off the equator, angled relative to the equator such that maximal depth is closer to the equator in the west. Substantial hemispheric asymmetry also stands out, with the southern deepening greater and wider. Mean Ztc in a combined ensemble of CMIP5 and CMIP6 models (MEM) is shown in Fig. 1b.

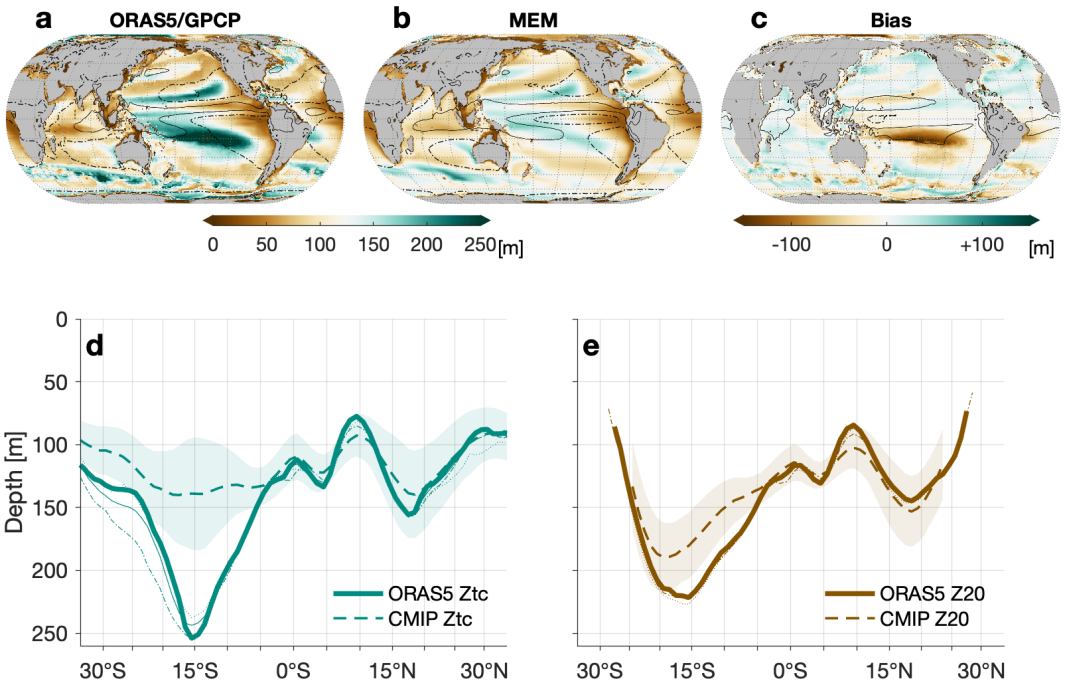

Figure 1. Annual mean thermocline depth (Ztc, color contours) and precipitation (line contours) in (**a**) observations (ORAS5 and GPCP), (**b**) CMIP model ensemble mean (MEM), and (**c**) MEM bias. Solid (dash-dotted) precipitation contours indicate values greater (smaller) than 3 mm day^{-1} in panels (a,b) and 1.5 mm day^{-1} in panel (c). (**d**) Thermocline depth and (**e**) 20°C isotherm depth (Z20) in the Pacific (160-260°E) in ORAS5 (thick solid), ORAS4 (thin solid), GODAS (dotted), SODA (dash-dotted) and MEM (dashed) with one standard deviation of the ensemble (shaded). All data is averaged from 1979–2005. To avoid seasonal biasing, Z20 is truncated poleward of ∼25° due to (hemispheric) summer surfacing.

The subtropical Pacific deepening in models is severely less pronounced and less hemispherically asymmetric, producing a mild bias in the northern hemisphere (NH) but an acute bias in the southern hemisphere (SH) (Fig. 1c). A similar southern bias of slightly lesser intensity is found in the south western Atlantic. We hereafter focus our analysis on the tropical Pacific, but note that the key elements of the shallow thermocline bias exist in the Atlantic, with unique features owing to the dynamic differences between the basins, which are beyond the scope of this work.

Pacific zonal mean Ztc and Z20 are shown in Figs. 1d and 1e, respectively. The observed thermocline is shallow in the subtropics, reaches maximal depth around 15° off the equator and shoals from there equatorward. The exception to this pattern is the NH shoaling around 9°N, just poleward of the ITCZ, caused by wind-driven divergent meridional currents. Hemispheric asymmetry is clearly observed, with over 100 meters differentiating the deepest southern point from the deepest northern point, leading to a tropical Pacific asymmetry index of $A_{\mathrm{Ztc}} = -0.32$. Z20 exhibits all of these features as well, with a similar asymmetry index of $A_{\mathrm{Z20}} = -0.31$. Equatorward of 10° Z20 deviates minimally from Ztc. However, poleward of this, Z20 is generally shallower than Ztc and diverges from Ztc completely as it surfaces poleward of ∼25–35° (depending on the season).

Biases in the NH are generally insignificant, perhaps with the exception of a mild deepening bias in the vicinity of the ITCZ (Zhu et al., 2021). In contrast with observations, the thermocline in models is significantly more flat and hemispherically symmetric, with a mean modeled A_{Ztc} value of -0.11. A robust bias is seen between 5°–30°S, which reaches over 100 meters at the deepest point of the observed thermocline. Inter-model spread is also maximal at this point, reaching a standard deviation of 50 meters. A similar but weaker bias is found in Z20, with model $A_{\mathrm{Z20}} = -0.15$. The biased region is also where Z20 and and Ztc diverge most, but in opposite directions in observation and models. Since Z20 is deeper than Ztc in models, but shallower than Ztc in observations, temperature at Ztc is distinctly warmer in models than in observations as a result of the shallow bias. We note that the bias in Ztc is not seasonal (Fig. S1a); SH Z20 seasonal variance is very weak in observations, and even more so in models (Fig. S1b).

To further understand the spatial structure of the thermocline bias, Fig. 2a shows meridional averages over equatorial and sub-equatorial sections (5°N–5°S, and 10°–20° in each hemisphere). The southern bias is pan-Pacific, and in proportion to thermocline depth, such that

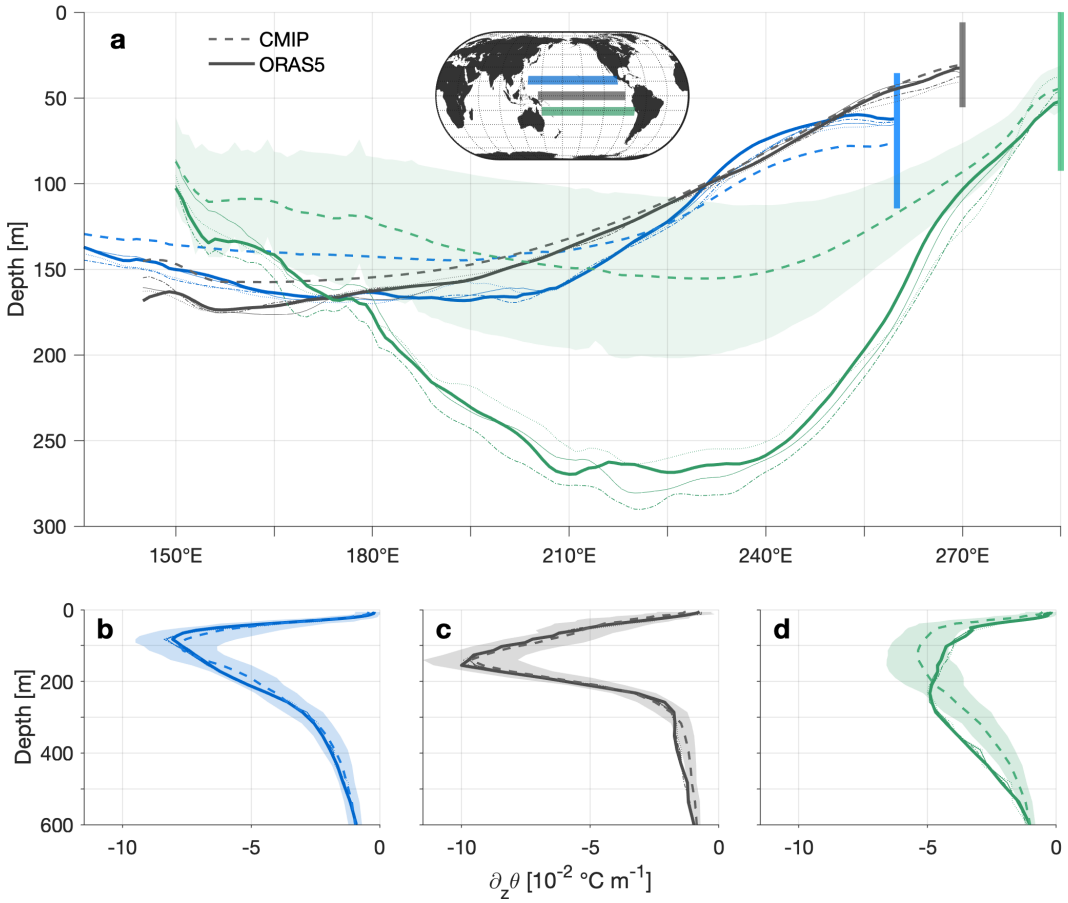

Figure 2. (**a**) Thermocline depth meridionally averaged in northern (10-20°N, 130-260°E, blue), equatorial (5°S-5°N, 145-270°E, grey) and southern (10-20°S, 150-285°E, green) sections, as marked in colors on the inset map. Vertical lines indicate the maximal span of ±1 standard deviation of model spread within the averaging region for each section. (**b**,**c**,**d**) Vertical potential temperature gradient, averaged meridionally and zonally over the sections shown in (a). The mixed layer at the top is imperceptible because of low vertical resolution. Datasets are denoted as in Fig. 1(d,e).

modeled zonal thermocline sloping is too weak. The NH and equatorial sections also have weak modelled zonal gradients, though both the observed gradient and the bias in it are smaller. As a result, zonal thermocline sloping is equivalent in all three sections in models. A similar but weaker bias is seen in Z20 in the southern section, which is further extended to the west relative to Ztc, since Z20 does not shoal in the west as Ztc does (Fig. S2a; Wang et al., 2000).

Figures 2b–d show vertical profiles of the vertical potential temperate gradient for the equatorial and sub-equatorial sections. The thermocline in the equatorial and NH sections is on average stronger and narrower than that of the SH, in models and observations alike. In the SH section, in addition to the shallow bias, the modeled thermocline is narrower than observed. This is true in section mean (Fig. 2d), as well as locally within it (Fig. S2b-g). No clear bias is seen in the strength of the thermocline. This is surprising, as one might expect a shallower and narrower thermocline to be less diffuse (Vallis, 2017). It is curious that while the modeled thermocline is more symmetric about the equator than observed, its strength is as asymmetric as in observations. This may point to surface rather than internal ocean processes at play. More significant positive biases in thermocline strength are found closer to the equator where the thermocline shoals (Fig. S3).

4 Inter-Model variance

To characterize the climate state associated with the shallow thermocline bias, in Fig. 3 we partition the ensemble, identifying the 10 models with the largest thermocline bias (shallowest thermocline) and smallest bias (deepest thermocline) in the 10-20°S section within the Pacific (160-260°E), where model spread is largest (Fig. 1d). The results are not sensitive to this particular range, nor to the number of models or to specific ensemble members, and nearly equal representation of CMIP5 and CMIP6 is found in both end member groups (see Tables T1/2). We find that the shallow thermocline models have a ridged southern thermocline, while the deep thermocline models have the observed southern dip, albeit not quite as pronounced (Fig. 3a). Accordingly, the ridged models have very weak asymmetry, while in dipped models $A_{\mathrm{Ztc}} = -0.22$, still significantly lower than observations. The ridged thermocline models have a shallower thermocline across the tropical Pacific; however, a large and robust bias is only found in the SH.

Precipitation in the ridged models has a stronger southern ITCZ bias, wider separation of precipitation peaks, and near zero asymmetry (Fig. 3c). In contrast, dipped models have a

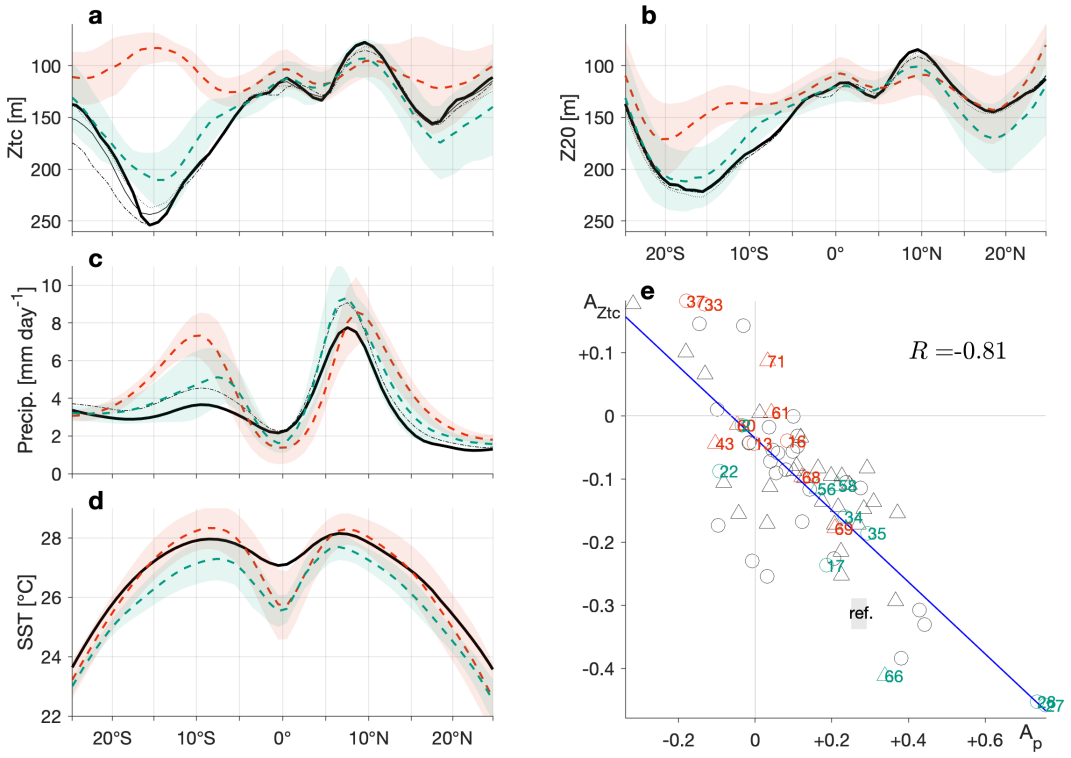

Figure 3. (**a**) Thermocline depth (Ztc), (**b**) 20°C isotherm depth (Z20), (**c**) precipitation, and (**d**) sea surface temperature for observations (black; a,b: see Fig. 1(d,e) for notation of datasets; c: GPCP (solid), CMAP (dash-dotted); e: ERSST), and mean of "ridged" models (red), and of "dipped" models (turquoize) (see text for partitioning), with ± 1 inter-model standard deviation (shaded). (**e**) Relation of precipitation (A_p) and thermocline (A_{Ztc}) asymmetry indices: grey rectangle gives observed range; circles and triangles denote CMIP5 and CMIP6 models, respectively, colors correspond to the model groups in (a-d) and numbers correspond to Tables T1/2. All quantities are averaged in the Pacific sector (160-260°E).

precipitation asymmetry index of 0.28, similar to the mean observed value (0.27). A close relation is found between asymmetry of thermocline depth and of precipitation (Fig. 3e), with correlation for the full ensemble of models $R = -0.81$, stronger than that found between precipitation and Z20 asymmetry ($R = -0.75$) or precipitation and SST asymmetry ($R = 0.76$). Of 73 models in the CMIP ensemble, only four have greater thermocline asymmetry than observations.

Dipped models have a tropical-wide cold SST bias (Fig. 3d), consistent with a generally deeper thermocline. The equatorial cold tongue region has a cold bias in both ensemble members; however, the off-equatorial meridional SST gradient is much larger in ridged models than in dipped ones or in observations. The resultant stronger cold tongue is consistent with a shallow equatorial thermocline bias (Zheng et al., 2012). Also in agreement with these results, off-equatorial meridional SST gradients have been shown to be as important to surface convergence and ITCZ formation as SST itself (Back & Bretherton, 2009). Moreover, the ridged models are asymmetrically warmer just south of the equator, creating an asymmetry bias in SST gradients that promotes south-equatorial deep convection and a DIB (Zhou et al., 2020).

Ridging is not seen to the same extent in Z20 (Fig. 3b). Instead, Ztc ridging is expressed in Z20 as a flattening in place of deepening. Nonetheless, lack of asymmetry is nearly as great in Z20 of the ridged thermocline, with $A_{Z20} = -0.10$. Z20 has no southern bias in the dipped group, though its hemispheric asymmetry is reduced relative to observations ($A_{Z20} = -0.18$). The temperature at the thermocline is therefore unbiased in the dipped group, whereas the southern thermocline is too warm in the ridged group. Lack of ridging in Z20 in the south may indicate a fundamental difference relative to the northern ridging (see discussion).

Shown in Fig. 4a, a strong separation between the groups emerges in SH thermocline zonal sloping, which is nearly as large in the dipped group as in observations. In contrast, a zonal slope is practically absent in the ridged group, to the point that thermocline asymmetry becomes positive westward of 230°E (compare to Fig. S4a). But even the dipped group exhibits only a mild degree of western shoaling, possibly related to a westward extended cold tongue and resultant warm pool cooling. Vertically, the thermocline is thicker and deeper in observations than in either group, with the ridged group most narrow (Fig. 4b). Thermocline strength does not have a clear bias among models, further questioning the role of stability (see text related to Fig. 2d).

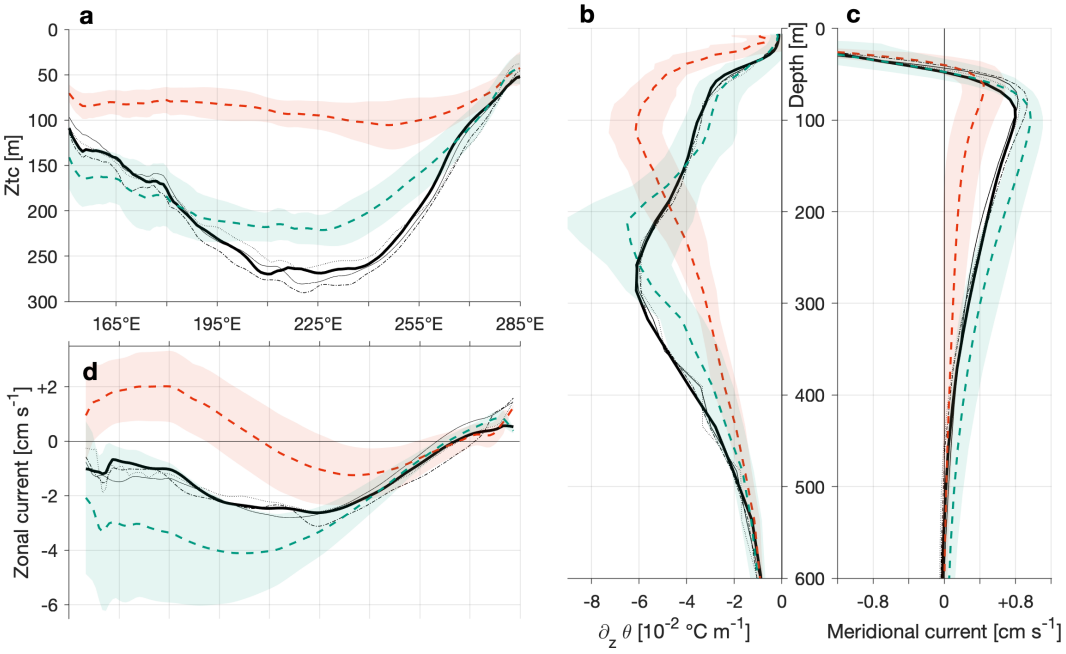

Figure 4. (**a**) Thermocline depth (*Ztc*) (10-20°S). ((**b**) Vertical potential temperature gradient and (**c**) Meridional current (10-20°S, 200-250°E). (**d**) Zonal current (8-13°S, upper 600 meter vertical mean). Datasets denoted as in Fig. 3(a,b).

Meridional current velocity in the region of 10-20°S and 200-250°E, is shown in Fig. 4c. Near surface poleward currents (outside the plotted range) are larger in the ridged models than in the dipped models or observations. The current changes direction from southward to northward around a depth of 40 meters in both groups of models and in reanalyses. The lower branch equatorward current in the ridged group is significantly weaker than the dipped group or observations, consistent (through geostrophy) with the weaker thermocline deepening slope to its left (west) in Fig. 4a. This weakening is also consistent with current velocities becoming much smaller below the thermocline: the northward return current reaches half of its maximal magnitude at a depth of ∼140 meters in the ridged group, ∼270 meters in the dipped group and ∼230 meters in observations. The meridional velocity bias may therefore be interpreted as a shrinking of the lower branch of the southern subtropical cell (Schott et al., 2004), which in turn may indicate altered ocean energy transport (Held, 2001).

In observations, northward displacement of the ITCZ and resultant southerly cross-equatorial wind drive the eastward north equatorial counter current, situated between the ITCZ and the equator (Vallis, 2017); but the SH and equatorial zonal surface currents are westward. In contrast with observations, ridged models have an eastward south equatorial counter current (SECC)

in the western Pacific between 8-13°S (Fig. 4d). Shoaling of the thermocline south of the SECC is expected, and thus so is a ridged thermocline. Consistent with Zhang & Song (2010), who found a similar spurious SECC in the NCAR CCSM3 model, this bias can be tied to a southward meridional wind stress bias (Fig. S5), associated with a southern ITCZ, through Ekman coupling.

5 Discussion and Conclusions

It is well known that the double ITCZ bias (DIB) has accompanying SST, surface wind and cloud radiative biases (Lin, 2007; Li & Xie, 2014; Zhang et al., 2019). However, to understand the fully coupled nature of these biases requires an understanding of their three-dimensional oceanic expression. Here we show that a significant southern shallow thermocline bias is a prominent feature of the tropical Pacific problem, and is equally present in both CMIP5 and CMIP6 models. The bias is manifested in both the physical thermocline (Ztc, the depth of maximal vertical temperature gradient) and the commonly-used 20°C isotherm, but is significantly more pronounced in Ztc. The bias is spatially coincident with precipitation biases, as evident in Fig. 1c, and its severity increases with the severity of the DIB (Fig. 3). Since water mass within the equatorial Pacific thermocline largely originates from the SH (Goodman et al., 2005), the southern Pacific shallow thermocline bias is a likely culprit of equatorial biases as well.

The key properties of the thermocline bias are:

1. A shallow bias between 5-30°S (Fig. 1d) and 160-260°E (Fig. 2a), up to 100 meters in ensemble mean.
2. Weak inter-hemispheric thermocline asymmetry ($A_{\mathrm{Ztc}} = -0.11$ in models compared to -0.32 in observations).
3. Thermocline and precipitation tropical asymmetry indices are strongly correlated ($R = -0.81$, Fig. 3e).

Features unique to the most severely biased models are the:

1. Ridged thermocline south of the equator (Fig. 3a),
2. Lack of zonal thermocline sloping (Fig. 4a),
3. Wider and stronger double ITCZ (Fig. 3c),
4. Warmer southern off-equatorial SST (Fig. 3d),
5. Stronger cold tongue (Fig. 3d),

6. Reduced meridional return current (Fig. 4c), and
7. Spurious south equatorial counter current (SECC, Fig. 4d).

Extensive work done related to the DIB over two and a half decades since it was first recognized by Mechoso et al. (1995), has treated it nearly exclusively in the annual mean. However, as Mechoso et al. (1995) and subsequent works pointed to, (e.g., De Szoeke & Xie, 2008; Li & Xie, 2014; Adam, Schneider, & Brient, 2018) this bias has distinct seasonal aspects, which peak in boreal spring. Thus, mechanisms that might explain the bias must account for its seasonality. In particular, mixed layer depth, and to a large extent tropical thermocline depth, which determine the thermal inertia of tropical waters on seasonal timescales, can modulate the seasonal amplitude of ITCZ migrations. Indeed, slab ocean experiments showed that ITCZ seasonal migration off the equator has a larger amplitude for shallower mixed layer depths (Donohoe et al., 2014). Moreover, to be convinced of the importance of thermal inertia to ITCZ migrations one need not look any further than the zonal variation in the extent to which the ITCZ travels meridionally on seasonal time scales, in direct relation to the zonal sloping of the Pacific thermocline. A smaller mass of water active in seasonal radiative heating and cooling will result in low thermal inertia, leading to (1) SST more easily increasing above the threshold required for deep convection, and (2) the latitude of maximal SST migrating further poleward. In this sense, a shallow thermocline is as much a condition for deep convection as it is a result of it (Knauss & Garfield, 2016). This mechanism offers a seasonal link between the DIB and the shallow thermocline bias, as it suggests that the summer hemisphere thermocline depth is the relevant variable to setting seasonal ITCZ migration.

The SECC, found here to be associated with thermocline ridging, has been suggested by Zhang & Song (2010) to be part of a positive feedback: the erroneous eastward current carries warm water from the western warm pool eastward, heating southeastern SST and promoting south-equatorial deep convection, a southern ITCZ and southward cross equatorial wind, which further strengthens the SECC through Ekman coupling. This mechanism is consistent with the SECC (Fig. 4d) and thermocline ridging (Fig. 4d) found here, concentrated in the western Pacific (Compare S6a and S6c). Interestingly, the spurious southern Ztc ridging is absent in Z20 (see text related to Fig. 3b). Local shoaling of Z20 and Ztc can result from positive wind stress curl, which leads to surface current divergence. Conversely, surface warming can lead to opposite trends in Ztc and Z20: deepening of Z20 because of overall warming of the upper ocean, but shoaling of Ztc, if the top part of the thermocline layer heats more than its

bottom part (Yang & Wang, 2009). This is the case, for example, in the western Pacific warm pool, where Ztc shoals significantly but Z20 does not (compare Fig. 2a to Fig. S2a). In the case of southern off-equatorial ridging, eastern Pacific Ztc shoals but does not ridge (Fig. S6a,b); but both western Pacific Ztc and Z20 exhibit ridging (Fig. S6c,d). This may indicate that the ridging biases originate from erroneous positive wind stress curl in the western Pacific, and translate to eastern biases through the resultant SECC, which carries heat to the southeastern Pacific.

Thermocline structure is influenced not only by local atmospheric forcing, but by independent resolved and unresolved ocean processes. Representation of turbulent mixing in ocean models in particular remains a major challenge (Guilyardi et al., 2009) and is critical to thermocline properties, their relation to SST and the positive feedback between wind strength, SST and the position of the ITCZ that maintains hemispheric asymmetry (S.-P. Xie & Philander, 1994). It follows that the thermocline bias might develop regardless of atmospheric biases. The evidence presented in this paper begs the questions: What part of the bias is set by atmospheric forcing? And to what extent does thermocline depth determine the tropical precipitation distribution?

One limitation of our results is the isolated treatment of the thermocline, without addressing salinity gradients and the resulting, possibly divergent, pycnocline. Though salinity gradients are mild in most of the tropics, heavy precipitation areas, such as the western warm pool can cause extreme surface freshening and a strong halocline, shallower than the thermocline. This results in a shallow pycnocline above the thermocline and a barrier layer between the two that further prevents mixing and entrainment from below (Sprintall & Tomczak, 1992; Breugem et al., 2008). Salinity can thus affect both the thermocline itself and the importance we attribute to it. Since we find significant precipitation biases in the thermocline bias region, and resultant salinity biases are known to exist (Zhi et al., 2019), salinity may be important, and should be addressed in future work. With that said, the thermal profile of the ocean column has important ramifications in and of itself, for mean ocean heat transport when combined with velocity fields, and for the local heat budget, just to name two.

To conclude, a clear connection is found here between the shallow thermocline bias in the southern Pacific and the well-known double ITCZ bias. Possible positive feedbacks among these include:

1. A shallow thermocline reduces thermal inertia, causing the ITCZ to more easily develop south of the equator, which creates wind convergence and Ekman current divergence at the ITCZ, further shoaling the thermocline (Donohoe et al., 2014).
2. Wind anomalies associated with the southward position of the ITCZ in models lead to a spurious SECC and shoaling south of it. This, in turn, causes eastward heat advection which reinforces the southward shift of the ITCZ and maintains a SECC and shoaled thermocline (Zhang & Song, 2010)

Ramifications of this bias to the fidelity of model predictions are potentially extensive. The dynamic and thermodynamic feedbacks mentioned here therefore merit further exploration.

Acknowledgments

The research was supported by the Israeli Science Foundation grant 1185/17. We thank Itamar Yacoby, Moran Erez and Eilat Elbaum for their helpful comments along the process. All of the data used in the analysis presented here is publicly available. We thank the climate modeling groups for producing and making available their model output, the Earth System Grid Federation (ESGF) for archiving the data and providing access, and the multiple funding agencies who support CMIP and ESGF. All CMIP data analyzed here are available from the ESGF at https://esgf-node.llnl.gov/projects/esgf-llnl.

References

Adam, O., Grise, K. M., Staten, P., Simpson, I. R., Davis, S. M., Davis, N. A., … Ming, A. (2018). The TropD software package (v1): standardized methods for calculating tropical-width diagnostics. *Geoscientific Model Development*, *11*(10), 4339–4357.

Adam, O., Schneider, T., & Brient, F. (2018). Regional and seasonal variations of the double-ITCZ bias in CMIP5 models. *Climate dynamics*, *51*(1-2), 101–117.

Adler, R. F., Huffman, G. J., Chang, A., Ferraro, R., Xie, P.-P., Janowiak, J., … others (2003). The version-2 global precipitation climatology project (GPCP) monthly precipitation analysis (1979–present). *Journal of hydrometeorology*, *4*(6), 1147–1167.

Back, L. E., & Bretherton, C. S. (2009). On the relationship between SST gradients, boundary layer winds, and convergence over the tropical oceans. *Journal of Climate*, *22*(15), 4182–4196.

Behringer, D., & Xue, Y. (2004). Evaluation of the global ocean data assimilation system at

NCEP: The Pacific Ocean. In *Proc. eighth symp. on integrated observing and assimilation systems for atmosphere, oceans, and land surface.*

Boccaletti, G., Pacanowski, R. C., George, S., Philander, H., & Fedorov, A. V. (2004). The thermal structure of the upper ocean. *Journal of physical oceanography*, *34*(4), 888–902.

Breugem, W.-P., Chang, P., Jang, C., Mignot, J., & Hazeleger, W. (2008). Barrier layers and tropical atlantic SST biases in coupled GCMs. *Tellus A: Dynamic Meteorology and Oceanography*, *60*(5), 885–897.

Burls, N. J., Muir, L., Vincent, E. M., & Fedorov, A. (2017). Extra-tropical origin of equatorial Pacific cold bias in climate models with links to cloud albedo. *Climate Dynamics*, *49*(5-6), 2093–2113.

Carton, J. A., Chepurin, G. A., & Chen, L. (2018). SODA3: A new ocean climate reanalysis. *Journal of Climate*, *31*(17), 6967–6983.

Castaño-Tierno, A., Mohino, E., Rodríguez-Fonseca, B., & Losada, T. (2018). Revisiting the CMIP5 thermocline in the equatorial Pacific and Atlantic oceans. *Geophysical Research Letters*, *45*(23), 12–963.

De Szoeke, S. P., & Xie, S.-P. (2008). The tropical eastern Pacific seasonal cycle: Assessment of errors and mechanisms in IPCC AR4 coupled ocean–atmosphere general circulation models. *Journal of Climate*, *21*(11), 2573–2590.

Donohoe, A., Frierson, D. M., & Battisti, D. S. (2014). The effect of ocean mixed layer depth on climate in slab ocean aquaplanet experiments. *Climate dynamics*, *43*(3-4), 1041–1055.

Fiedler, P. C. (2010). Comparison of objective descriptions of the thermocline. *Limnology and Oceanography: Methods*, *8*(6), 313–325.

Goodman, P. J., Hazeleger, W., de Vries, P., & Cane, M. (2005). Pathways into the Pacific Equatorial Undercurrent: A trajectory analysis. *Journal of physical oceanography*, *35*(11), 2134–2151.

Guilyardi, E., Wittenberg, A., Fedorov, A., Collins, M., Wang, C., Capotondi, A., … Stockdale, T. (2009). Understanding El Niño in ocean–atmosphere general circulation models: Progress and challenges. *Bulletin of the American Meteorological Society*, *90*(3), 325–340.

Harper, S. (2000). Thermocline ventilation and pathways of tropical–subtropical water mass exchange. *Tellus A: Dynamic Meteorology and Oceanography*, *52*(3), 330–345.

Held, I. M. (2001). The partitioning of the poleward energy transport between the tropical

ocean and atmosphere. *Journal of the Atmospheric Sciences*, *58*(8), 943–948.

Hwang, Y.-T., & Frierson, D. M. (2013). Link between the double-intertropical convergence zone problem and cloud biases over the Southern Ocean. *Proceedings of the National Academy of Sciences*, *110*(13), 4935–4940.

Knauss, J. A., & Garfield, N. (2016). *Introduction to physical oceanography*. Waveland Press.

Li, G., & Xie, S.-P. (2012). Origins of tropical-wide SST biases in CMIP multi-model ensembles. *Geophysical research letters*, *39*(22).

Li, G., & Xie, S.-P. (2014). Tropical biases in CMIP5 multimodel ensemble: The excessive equatorial Pacific cold tongue and double ITCZ problems. *Journal of Climate*, *27*(4), 1765–1780.

Lin, J.-L. (2007). The double-ITCZ problem in IPCC AR4 coupled GCMs: Ocean–atmosphere feedback analysis. *Journal of Climate*, *20*(18), 4497–4525.

Luyten, J., Pedlosky, J., & Stommel, H. (1983). The ventilated thermocline. *Journal of Physical Oceanography*, *13*(2), 292–309.

Mechoso, C. R., Robertson, A. W., Barth, N., Davey, M., Delecluse, P., Gent, P., ... others (1995). The seasonal cycle over the tropical pacific in coupled ocean–atmosphere general circulation models. *Monthly Weather Review*, *123*(9), 2825–2838.

Schott, F. A., Mccreary, J. P., & Johnson, G. C. (2004). Shallow overturning circulations of the tropical-subtropical oceans. *Earth Climate: The Ocean–Atmosphere Interaction, Geophys. Monogr*, *147*, 261–304.

Smith, T. M., Reynolds, R. W., Peterson, T. C., & Lawrimore, J. (2008). Improvements to NOAAâs historical merged land–ocean surface temperature analysis (1880–2006). *Journal of Climate*, *21*(10), 2283–2296.

Sprintall, J., & Tomczak, M. (1992). Evidence of the barrier layer in the surface layer of the tropics. *Journal of Geophysical Research: Oceans*, *97*(C5), 7305–7316.

Sverdrup, H. U., Johnson, M. W., Fleming, R. H., et al. (1942). *The Oceans: Their physics, chemistry, and general biology* (Vol. 7). Prentice-Hall New York.

Thomas, M. D., & Fedorov, A. V. (2017). The eastern subtropical Pacific origin of the equatorial cold bias in climate models: A Lagrangian perspective. *Journal of Climate*, *30*(15), 5885–5900.

Vallis, G. K. (2017). *Atmospheric and oceanic fluid dynamics*. Cambridge University Press.

Vialard, J., Menkes, C., Boulanger, J.-P., Delecluse, P., Guilyardi, E., McPhaden, M. J., &

Madec, G. (2001). A model study of oceanic mechanisms affecting equatorial Pacific sea surface temperature during the 1997–98 El Niño. *Journal of Physical Oceanography*, *31*(7), 1649–1675.

Wang, B., Wu, R., & Lukas, R. (2000). Annual adjustment of the thermocline in the tropical Pacific Ocean. *Journal of Climate*, *13*(3), 596–616.

Xie, P., & Arkin, P. A. (1996). Analyses of global monthly precipitation using gauge observations, satellite estimates, and numerical model predictions. *Journal of climate*, *9*(4), 840–858.

Xie, S.-P., & Philander, S. G. H. (1994). A coupled ocean-atmosphere model of relevance to the ITCZ in the eastern Pacific. *Tellus A*, *46*(4), 340–350.

Yang, H., & Wang, F. (2009). Revisiting the thermocline depth in the equatorial Pacific. *Journal of Climate*, *22*(13), 3856–3863.

Zhang, G. J., & Song, X. (2010). Convection parameterization, tropical Pacific double ITCZ, and upper-ocean biases in the NCAR CCSM3. Part II: Coupled feedback and the role of ocean heat transport. *Journal of Climate*, *23*(3), 800–812.

Zhang, G. J., Song, X., & Wang, Y. (2019). The double ITCZ syndrome in GCMs: A coupled feedback problem among convection, clouds, atmospheric and ocean circulations. *Atmospheric Research*.

Zheng, Y., Lin, J.-L., & Shinoda, T. (2012). The equatorial Pacific cold tongue simulated by IPCC AR4 coupled GCMs: Upper ocean heat budget and feedback analysis. *Journal of Geophysical Research: Oceans*, *117*(C5).

Zhi, H., Zhang, R.-H., Lin, P., & Yu, P. (2019). Interannual salinity variability in the tropical pacific in CMIP5 simulations. *Advances in Atmospheric Sciences*, *36*(4), 378–396.

Zhou, S., Huang, G., & Huang, P. (2020). Excessive ITCZ but negative SST biases in the tropical Pacific simulated by CMIP5/6 models: The role of the meridional pattern of SST bias. *Journal of Climate*, *33*(12), 5305–5316.

Zhu, Y., Zhang, R.-H., Li, D., & Chen, D. (2021). The thermocline biases in the tropical North Pacific and their attributions. *Journal of Climate*, *34*(5), 1635–1648.

Zuo, H., Balmaseda, M. A., Tietsche, S., Mogensen, K., & Mayer, M. (2019). The ECMWF operational ensemble reanalysis–analysis system for ocean and sea ice: a description of the system and assessment. *Ocean science*, *15*(3), 779–808.